PASJ: Publ. Astron. Soc. Japan **63**, S751–S757, 2011 November 25

Discovery of a Cyclotron Resonance Feature in the X-Ray Spectrum of GX 304−1 with RXTE and Suzaku during Outbursts Detected by MAXI in 2010

Takayuki YAMAMOTO,[1,2] Mutsumi SUGIZAKI,[2] Tatehiro MIHARA,[2] Motoki NAKAJIMA,[3] Kazutaka YAMAOKA,[4] Masaru MATSUOKA,[2] Mikio MORII,[5] and Kazuo MAKISHIMA[2,6]

[1]*Department of Physics, Nihon University, 1-8-14 Surugadai, Chiyoda-ku, Tokyo 101-8308*
tyamamot@crab.riken.jp
[2]*MAXI team, RIKEN, 2-1 Hirosawa, Wako, Saitama 351-0198*
[3]*School of Dentistry at Matsudo, Nihon University, 2-870-1 Sakaecho-nishi, Matsudo, Chiba 101-8308*
[4]*Department of Physics and Mathematics, Aoyama Gakuin University, 5-10-1 Fuchinobe, Chuo-ku, Sagamihara 252-5258*
[5]*Department of Physics, Tokyo Institute of Technology, 2-12-1 Ookayama, Meguro-ku, Tokyo 152-8551*
[6]*Department of Physics, The University of Tokyo, 7-3-1 Hongo, Bunkyo-ku, Tokyo 113-0033*

(Received 2010 December 9; accepted 2011 February 21)

Abstract

We report on the discovery of a cyclotron resonance scattering feature (CRSF) in the X-ray spectrum of GX 304−1, obtained by RXTE and Suzaku during major outbursts detected by MAXI in 2010. The peak intensity in August reached 600 mCrab in the 2–20 keV band, which is the highest ever observed from this source. The RXTE observations on more than twenty occasions and one Suzaku observation revealed a spectral absorption feature at around 54 keV, which is the first CRSF detection from this source. The estimated strength of the surface magnetic field, 4.7×10^{12} G, is one of the highest among binary X-ray pulsars from which CRSFs have ever been detected. The RXTE spectra taken during the August outburst also suggest that the CRSF energy changed over 50–54 keV, possibly in a positive correlation with the X-ray flux. The behavior is qualitatively similar to that observed from Her X-1 on long time scales, or from A 0535+26, but different from the negative correlation observed from 4U 0115+63 and X 0331+53.

Key words: pulsars: individual (GX 304−1) — stars: magnetic fields — stars: neutron — X-rays: binaries

1. Introduction

The magnetic-field strength of neutron stars is one of the important parameters related to their fundamental physics. The surface magnetic field of accreting X-ray pulsars can be best estimated from the Cyclotron Resonance Scattering Feature (CRSF) in their X-ray spectra. The CRSFs have always been detected from 15 X-ray pulsars, and their surface magnetic fields are found to be distributed within a relatively narrow range of $(1–4) \times 10^{12}$ G (e.g., Trümper et al. 1978; White et al. 1983; Mihara 1995; Makishima et al. 1999; Coburn et al. 2002; and references therein).

GX 304−1 was discovered by high-energy X-ray balloon observations carried out since 1967 (e.g., McClintock et al. 1971). It exhibits properties typical of binary X-ray pulsars, including a large flux variability (Ricker et al. 1973), the 272-s coherent pulsation (Huckle et al. 1977; McClintock et al. 1977), and a hard X-ray spectrum represented by a power-law with an absorption column density of $N_{\rm H} \sim 1 \times 10^{22}$ cm^{-2} and a photon index of $\Gamma \sim 2$ up to 40 keV (White et al. 1983). A study with the Vela 5B satellite over a period of 7 years revealed a 132.5-day periodicity of flaring events (Priedhorsky & Terrell 1983), attributable to the binary period.

GX 304−1 has been identified with a Be star system (Mason et al. 1978), showing strong shell lines (Thomas et al. 1979; Parkes et al. 1980) and photometric variability (Menzies et al. 1981) in optical wavelengths. From a visual extension ($A_V = 6.9$ mag) to the source directions, the distance was estimated to be 2.4 ± 0.5 kpc (Parkes et al. 1980). Thus is consistent with the observed X-ray absorption column density (White et al. 1983).

Since 1980, GX 304−1 had been in an X-ray off state (Pietsch et al. 1986), and no significant X-ray emission was detected for 28 years. Its quiescence was broken by hard X-ray detection with INTEGRAL in 2008 June (Manousakis et al. 2008). Since then, the source seemed to return to the active state. Actually, from 2009 November to 2011 January, MAXI and Swift have detected three outbursts every 132.5-day interval (Yamamoto et al. 2009; Krimm et al. 2010; Mihara et al. 2010a).

We here report on the discovery of a CRSF in RXTE and Suzaku X-ray spectra of GX 304−1, obtained during the outbursts in 2010 through follow-up observations triggered by MAXI. We also discuss a possible change of the observed CRSF energy.

2. Observations and Data Reductions

2.1. Monitoring with MAXI

MAXI/GSC (Matsuoka et al. 2009; Mihara et al. 2011) has been monitoring the flux of GX 304−1 since the mission started (Sugizaki et al. 2011). Figure 1 shows the MAXI/GSC light curve of GX 304−1 from 2009 August 15 (MJD = 55058) to 2011 January 31 (MJD = 55592). Four outbursts were detected with an interval of 132.5 d, which is consistent with the orbital period suggested from the Vela 5B

Table 1. Log of RXTE observations of GX 304−1 in the 2010 August outburst.

Date	Obs ID	Obs time	PCA (3–20 keV)*		HEXTE (20–100 keV)	
(2010 Aug)	(95417-01-)	Start / End (UT)	Exposure (ks)	Rate (counts s^{-1})	Exposure (ks)	Rate (counts s^{-1})
13a	03-03	03:32 / 04:20	2.3	941.3 ± 1.1	1.4	147.6 ± 0.4
13b	03-00	04:44 / 06:37	3.7	997.9 ± 1.1	2.3	155.0 ± 0.3
14	03-01	01:37 / 04:35	5.4	1060.0 ± 1.1	1.5	163.9 ± 0.4
15	03-02	01:59 / 04:45	6.1	1143.0 ± 1.2	2.0	175.4 ± 0.3
18	04-00	02:25 / 03:57	3.3	1130.0 ± 1.3	2.1	163.9 ± 0.3
19	04-01	01:57 / 02:57	3.2	1211.0 ± 1.4	2.0	176.3 ± 0.4
20	05-00	00:02 / 01:00	3.2	1110.0 ± 1.3	1.9	159.6 ± 0.3
21	05-01	20:33 / 20:55	1.0	774.4 ± 1.2	0.6	101.6 ± 0.5
22	05-02	23:58 / 00:43	2.0	654.8 ± 0.9	1.2	82.9 ± 0.4
24	05-03	02:40 / 03:44	3.4	546.7 ± 0.7	2.1	64.1 ± 0.2
25	05-04	05:44 / 06:12	1.2	422.2 ± 0.7	0.9	48.1 ± 0.4
26	05-05	00:42 / 01:16	1.4	376.5 ± 0.7	0.8	44.6 ± 0.4

* PCU2 only.

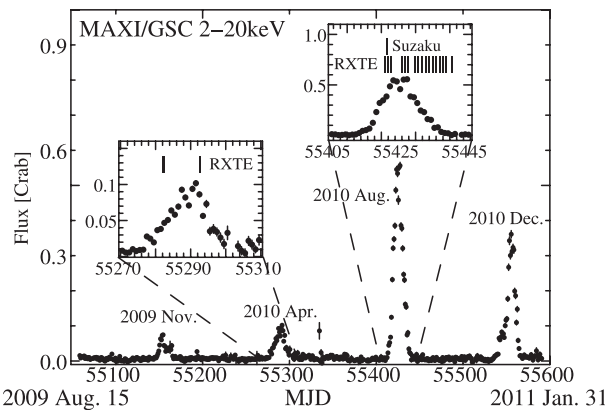

Fig. 1. MAXI/GSC light curve of GX 304−1 in the 2–20 keV band from 2009 August 15 to 2011 January 31. The left inset shows a zoom-up around the outburst from 2010 March 15 to April 24, and the right inset the outburst from 2010 July 28 to September 6. The RXTE and Suzaku observations are indicated with bars in each inset.

data (Priedhorsky & Terrell 1983). They peaked on 2009 November 19 (MJD = 55154), 2010 April 1 (MJD = 55287), 2010 August 15 (MJD = 55423), and 2011 December 25 (MJD = 55555). The peak intensities of the first three outbursts gradually increased. In the 2–20 keV band, the outburst in 2010 August reached 0.6 Crab, which is the highest among flaring events ever observed from this source. The 2010 December outburst was also bright, but did not reach the level of the 2010 August event.

2.2. *RXTE Observations*

RXTE ToO (Target of Opportunity) observations of GX 304−1 were performed during the outbursts in 2010 March and August, and gave useful data in the energy range from 3 to 250 keV with the Proportional Counter Array (PCA: Jahoda et al. 2006) and the High-Energy X-ray Timing Experiment (HEXTE: Rothschild et al. 1998). A total of 21 observations were carried out, with an exposure of 0.5–5 ks each. The observation epochs are indicated in figure 1.

The RXTE data were reduced with the standard procedure using the relevant analysis software in HEASOFT version 6.9 and CALDB (calibration database) files of version 20100607, provided by NASA/GSFC RXTE GOF (Guest Observer Facility). PCA source spectra and background files in the 3–20 keV energy band were extracted from layer1 in PCU 2 alone.

The hard X-ray (> 20 keV) spectra of the source were extracted from the HEXTE cluster-A, while backgrounds were extracted from cluster-B and converted to cluster-A background files using ftool hextebackest. Since the HEXTE background spectra reproduced by the standard method are known to have a relatively large calibration uncertainty at around 63 keV for the data after 2009 December,[1] we chose for a subsequent spectral analysis observations whose signal-to-background ratio is higher than 30% at 50 keV. Table 1 summarizes the log of the selected twelve observations.

2.3. *Suzaku Observation*

A Suzaku ToO observation of GX 304−1 was performed on 2010 August 13, two days before the outburst maximum. It was triggered by the MAXI detection of the rapid flux increase (Mihara et al. 2010a). The Suzaku data cover an energy band from 0.5 to 500 keV, using the X-ray Imaging Spectrometer (XIS: Koyama et al. 2007) and the Hard X-ray Detector (HXD: Takahashi et al. 2007; Kokubun et al. 2007). The target was placed at the HXD nominal position on the detectors. XIS was operated in the normal mode with 1/4-window and 0.5 s burst options, which gave a time resolution of 2 s. The HXD was operated in the nominal mode. Table 2 summarizes the observation log.

The data reduction and analysis were performed with the standard procedure using the Suzaku analysis software in HEASOFT version 6.9 and the CALDB files version 20100812, provided by NASA/GSFC Suzaku GOF. All

[1] ⟨http://heasarc.gsfc.nasa.gov/docs/xte/xhp_new.html⟩.

Table 2. Log of Suzaku observation of GX 304−1 in the 2010 August outburst.*

Date	Obs time	XIS 0 (1–10 keV)		HXD-PIN (15–75 keV)		HXD-GSO (50–130 keV)	
(2010 Aug)	Start / End (UT)	Exposure (ks)	Rate (counts s^{-1})	Exposure (ks)	Rate (counts s^{-1})	Exposure (ks)	Rate (counts s^{-1})
13	16:19 / 23:00	5.13	150.6 ± 0.2	12.14	36.25 ± 0.05	12.14	2.56 ± 0.05

* Observation ID = 905002010.

obtained data were first reprocessed by aepipeline to utilize the latest calibration. The net exposures after the standard event-screening process were 5.1 ks with the XIS and 12.1 ks with the HXD. The former is significantly shorter than the latter because of the 0.5 s burst option. The background spectra for HXD-PIN and HXD-GSO were created in the standard manner, using the archived background event files provided via the Suzaku GOF. This process also removed the Cosmic X-ray Background (CXB) from the HXD-PIN data, while that in the HXD-GSO data was negligible (Fukazawa et al. 2009). After subtracting the backgrounds, the source was detected significantly at an intensity of 36.3 ± 0.05 counts s^{-1} with PIN in 15–75 keV, and 2.46 ± 0.05 counts s^{-1} with GSO in 50–130 keV.

3. Analysis and Results

The barycentric pulsation period was derived to be 275.46 s during the Suzaku observation, from a folding analysis of the HXD-PIN data.

The RXTE and Suzaku observations both provide us with an opportunity to search for CRSFs that have not been detected from GX 304−1 in the X-ray energy band up to 40 keV (White et al. 1983). Hereafter, we concentrate on an analysis of the pulse-phase-averaged spectra for CRSFs.

We present results using the data of the PCA (3–20 keV) and the HEXTE (20–100 keV) from RXTE, and those of HXD-PIN (15–75 keV) and HXD-GSO (50–130 keV) from Suzaku. The Suzaku XIS data were not used in the present paper, because they suffer considerably from event pile-up. All of the spectral fits were carried out on XSPEC version 12.6.0.

3.1. CRSF in X-Ray Spectra by RXTE and Suzaku

We first performed joint spectral fits to the data taken by RXTE and Suzaku during 12 hours from August 13 16:00 (UT), as presented in figure 2. Since these observations were not exactly simultaneous, the average flux can be different between the two data sets. We thus introduced a parameter representing relative normalization of the over-all model, and allowed it to take defferent values among the PCA, HEXTE, HXD-PIN, and HXD-GSO spectra. The four values of this parameter agreed with one another within calibration uncertainties.

We here consider the validity of the RXTE-HEXTE background spectrum. The energy band from 61 keV to 71 keV was ignored in all subsequent analysis, since artificial structures are known to remain for the data taken after 2009 December. We also attempted to change the background scale factor, and checked if any artificial features remained in the residual. Assuming that there is no significant source flux above the background in a higher energy band of 150–250 keV,

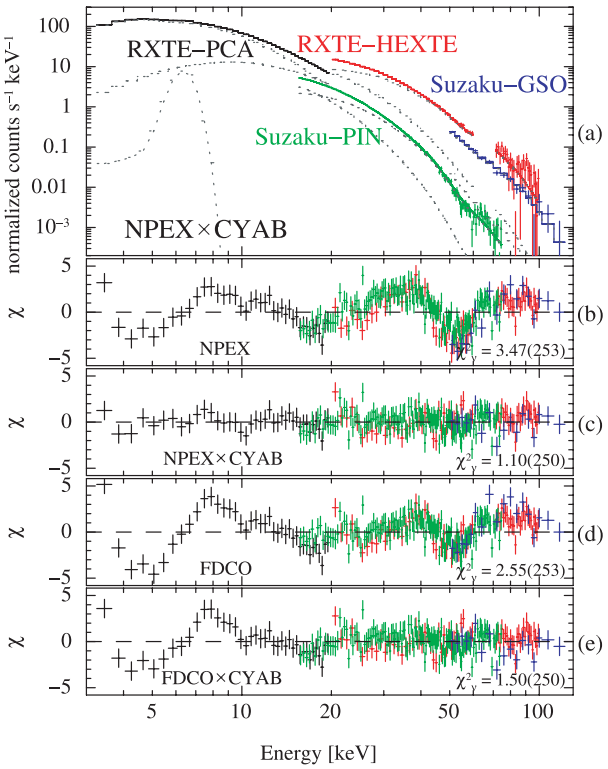

Fig. 2. X-ray spectra of GX 304−1 observed by RXTE and Suzaku on August 13–14. (a) Data and the best-fit spectral models of NPEX × CYAB. (b)–(e) Residuals from the best-fit NPEX, NPEX × CYAB, FDCO, and FDCO × CYAB models, respectively.

the best background scale factor was obtained to be 1.1. We employed this value when subtracting the HEXTE background. The validity was further confirmed from the consistency with the Suzaku data.

We employed a cutoff power-law (cutoffpl model in XSPEC), an NPEX (Negative and Positive power laws with exponential cutoff: Mihara 1995; Makishima et al. 1999) or an FDCO (Fermi-Dirac cutoff power-law: Makishima et al. 1999) model to reproduce the continuum from 3 keV to 130 keV. The cutoffpl model was far from successful, with reduced chi-squared $\chi^2_\nu = 16.8$ for degrees of freedom of $\nu = 254$. Thus, it was excluded in a following spectral analysis. In the NPEX model we left free all parameters but one: the positive power-law index, α_2, was fixed at 2.0, representing a Wien peak, because it was not well constrained by the data. The fit with either the NPEX or FDCO model alone was unacceptable ($\chi^2_\nu = 3.47$ for $\nu = 253$, and $\chi^2_\nu = 2.55$ for $\nu = 253$, respectively). As shown in figures 2b and 2d, the residuals similarly exhibit absorption features at around 20–30 keV and

Table 3. Summary of joint fits to Suzaku and RXTE spectra taken on 2010 August 13–14.*

Parameter	Model					
	cutoffpl	FDCO	FDCO×CYAB	NPEX	NPEX×CYAB	NPEX×CYAB2†
$N_{\rm H}$ (10^{22} cm^{-2})	0.00	5.93	$5.26^{+0.23}_{-0.24}$	4.22	$3.13^{+0.24}_{-0.26}$	$3.08^{+0.33}_{-0.23}$
$I_{\rm Fe}$‡ ($\times 10^{-2}$)	1.90	0.67	0.82 ± 0.13	0.81	0.91 ± 0.13	$0.91^{+0.13}_{-0.14}$
A_1§ ($\times 10^{0}$)	0.43	1.73	1.60 ± 0.05	0.92	0.72 ± 0.03	$0.71^{+0.03}_{-0.04}$
α_1	0.35	1.33	1.25 ± 0.02	0.57	0.49 ± 0.02	0.50 ± 0.02
$E_{\rm cut}$ (keV)	—	31.7	$27.7^{+0.9}_{-1.1}$	—	—	—
$kT/E_{\rm fold}$ (keV)	11.2	9.0	$11.8^{+0.7}_{-0.5}$	6.5	7.4 ± 0.2	$7.5^{+0.1}_{-0.2}$
A_2§ ($\times 10^{-4}$)	—	—	—	9.4	$5.2^{+0.5}_{-0.6}$	5.1 ± 0.8
$E_{\rm a1}$ (keV)	—	—	$54.5^{+1.1}_{-0.9}$	—	$53.7^{+0.7}_{-0.6}$	26.9 ± 0.3
W_1 (keV)	—	—	$9.8^{+2.9}_{-2.2}$	—	$10.2^{+2.3}_{-2.0}$	5.0 fixed
D_1	—	—	$0.75^{+0.13}_{-0.09}$	—	$0.73^{+0.09}_{-0.06}$	$0.01^{+0.02}_{-0.01}$
W_2 (keV)	—	—	—	—	—	$10.9^{+2.1}_{-2.4}$
D_2	—	—	—	—	—	$0.75^{+0.15}_{-0.08}$
χ^2_ν (ν)	16.8 (254)	2.55 (253)	1.50 (250)	3.47 (253)	1.10 (250)	1.10 (249)

* All errors represent the 90% confidence limits of the statistical uncertainties.
† CYAB2: $E_{\rm a2}$ energy is fixed to $2\,E_{\rm a1}$.
‡ Units in photons s^{-1} cm^{-2}.
§ Units in photons s^{-1} cm^{-2} keV^{-1} at 1 keV.

40–60 keV in both the RXTE and the Suzaku spectra, respectively.

We then multiplied the continuum models with cyclotron absorption (CYAB) factors (Mihara et al. 1990; Makishima et al. 1999). The NPEX model with a single CYAB feature was accepted within the 90% confidence limit ($\chi^2_\nu = 1.10$ for $\nu = 250$), as shown in figure 2c. The fundamental resonance energy was obtained to be $E_{\rm a} = 53.7^{+0.7}_{-0.6}$ keV. In contrast, the FDCO model with a CYAB was not acceptable ($\chi^2_\nu = 1.50$ for $\nu = 250$), leaving wavy residuals in 3–10 keV in figure 2e.

The NPEX model with two CYAB features that represent the fundamental harmonics $E_{\rm a1} \sim 20$ keV, and the second harmonics $E_{\rm a2} = 2E_{\rm a1}$ was also examined. However, the fit was not improved at all ($\chi^2_\nu = 1.10$ for $\nu = 249$) and the depth of the fundamental harmonic was zero within the statistical error. Therefore, both the RXTE and the Suzaku data confirm the presence of a fundamental CRSF at about $E_{\rm a} = 54$ keV, and imply that the NPEX continuum is most successful among the three models tested. Table 3 summarizes these fitting results and the best-fit model parameters. As given there, the FDCO model (though not acceptable) gives a consistent resonance energy.

3.2. *CRSF Energy Variation*

As shown in figure 1, the RXTE observations in 2010 August covered the peak-to-descent phase of the outburst on an almost daily basis. The data enable us to investigate spectral variations in this period.

With the same procedure as described in subsection 3.1, model fits to individual spectra taken in these RXTE observations and the Suzaku were performed. By artificially changing the HEXTE background by ±5% of the nominal value, we confirmed that the obtained best-fit parameters are not sensitive to the background uncertainty.

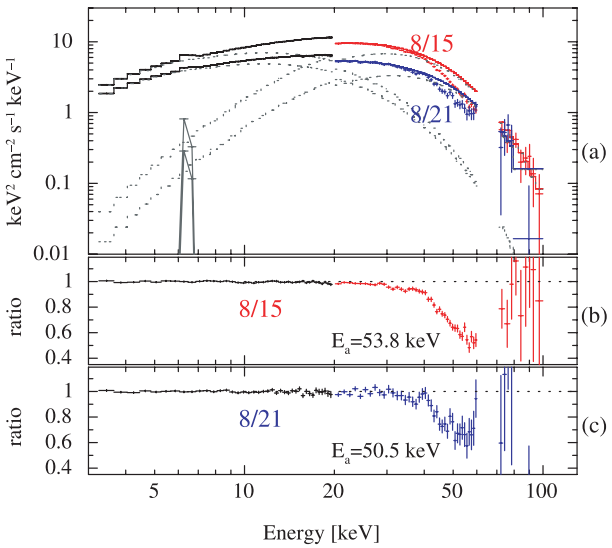

Fig. 3. Comparison of X-ray spectra taken by RXTE on August 15 and 21. (a) Unfolded spectra and best-fit NPEX×CYAB models. The negative and positive power-law components are shown by dotted lines. (b) Data-to-model ratio for the August 15 spectrum, shown after removing the CYAB factor from the best-fit NPEX×CYAB fit. (c) Same as (b), but for the August 21 spectrum.

These spectral fits with the NPEX model revealed that the CYAB feature is required by all of the spectra of the selected observations with a significance above 90%. The obtained best-fit parameters are summarized in table 4, where the CRSF energy is seen to vary, beyond the fitting errors, by $\sim 6\%$ among the observations. Figure 3 illustrates the difference of

Table 4. Best-fit parameters of the NPEX × CYAB models to spectra by RXTE and Suzaku in 2010 August outburst.

Date	$N_{\rm H}$ (10^{22} cm^{-2})	$I_{\rm Fe}$† ($\times 10^{-2}$)	A_1‡ ($\times 10^{0}$)	α_1	A_2‡ ($\times 10^{-5}$)	kT (keV)	$E_{\rm a}$ (keV)	W_1 (keV)	D_1	χ^2_ν (ν)	$L_{\rm x}$§
13a	$3.00^{+0.30}_{-0.31}$	$1.01^{+0.14}_{-0.13}$	0.69 ± 0.04	$0.49^{+0.02}_{-0.03}$	$56.5^{+6.3}_{-7.8}$	$7.2^{+0.3}_{-0.2}$	$53.0^{+1.4}_{-1.1}$	$7.4^{+3.5}_{-2.4}$	$0.67^{+0.09}_{-0.08}$	1.10 (98)	1.92
13b	$2.95^{+0.27}_{-0.29}$	$0.96^{+0.14}_{-0.13}$	$0.71^{+0.04}_{-0.06}$	0.47 ± 0.02	$58.6^{+5.3}_{-6.3}$	$7.2^{+0.2}_{-0.1}$	$52.4^{+0.8}_{-0.7}$	$6.5^{+2.3}_{-1.7}$	$0.65^{+0.07}_{-0.06}$	1.13 (98)	2.04
13**	—	—	$0.53^{+0.42}_{-0.20}$	$0.38^{+0.27}_{-0.20}$	$57.6^{+19.9}_{-11.8}$	7.2 ± 0.3	$53.8^{+0.8}_{-0.7}$	$7.4^{+2.4}_{-2.0}$	$0.75^{+0.09}_{-0.08}$	1.05 (146)	2.09
14	$2.94^{+0.27}_{-0.28}$	1.00 ± 0.04	0.74 ± 0.04	0.46 ± 0.02	$58.7^{+6.7}_{-8.8}$	$7.3^{+0.3}_{-0.2}$	$52.7^{+1.2}_{-0.9}$	$8.1^{+3.3}_{-2.5}$	$0.60^{+0.09}_{-0.07}$	0.96 (98)	2.16
15	$2.99^{+0.26}_{-0.27}$	1.20 ± 0.04	$0.78^{+0.04}_{-0.03}$	0.46 ± 0.02	$60.8^{+6.6}_{-8.7}$	$7.4^{+0.3}_{-0.2}$	$53.8^{+1.2}_{-1.0}$	$9.6^{+3.4}_{-2.5}$	$0.66^{+0.12}_{-0.07}$	0.97 (98)	2.33
18‖	$2.77^{+0.26}_{-0.27}$	$1.10^{+0.14}_{-0.15}$	0.79 ± 0.04	0.47 ± 0.02	$45.2^{+5.8}_{-7.0}$	$7.6^{+0.3}_{-0.2}$	$52.4^{+1.0}_{-0.8}$	$7.7^{+2.9}_{-2.1}$	$0.60^{+0.09}_{-0.06}$	0.86 (56)	2.24
19	2.32 ± 0.26	$1.33^{+0.15}_{-0.16}$	0.77 ± 0.04	0.43 ± 0.02	$42.7^{+6.8}_{-8.0}$	$7.7^{+0.4}_{-0.2}$	$51.8^{+0.8}_{-0.7}$	$8.1^{+2.9}_{-2.2}$	$0.56^{+0.10}_{-0.06}$	0.88 (98)	2.39
20	$2.83^{+0.25}_{-0.27}$	$1.14^{+0.14}_{-0.15}$	0.77 ± 0.04	0.47 ± 0.02	$39.0^{+5.1}_{-5.8}$	$7.7^{+0.3}_{-0.2}$	$51.3^{+0.8}_{-0.7}$	$6.0^{+2.4}_{-1.9}$	0.48 ± 0.06	1.19 (98)	2.19
21	$3.13^{+0.35}_{-0.34}$	0.42 ± 0.13	0.69 ± 0.04	0.59 ± 0.03	$22.5^{+5.6}_{-5.8}$	$7.9^{+0.5}_{-0.4}$	$50.5^{+1.8}_{-1.4}$	$6.0^{+4.5}_{-3.4}$	$0.52^{+0.16}_{-0.13}$	0.85 (98)	1.46
22	3.06 ± 0.29	0.56 ± 0.10	0.67 ± 0.03	$0.68^{+0.03}_{-0.02}$	$14.2^{+3.1}_{-2.9}$	$8.3^{+0.4}_{-0.2}$	$49.6^{+0.8}_{-0.7}$	$4.3^{+2.2}_{-1.9}$	$0.79^{+0.24}_{-0.16}$	0.97 (98)	1.21
24	3.39 ± 0.26	0.31 ± 0.08	0.62 ± 0.03	0.74 ± 0.03	9.7 ± 1.9	$8.5^{+0.3}_{-0.1}$	$50.9^{+1.4}_{-1.1}$	$6.3^{+3.0}_{-2.2}$	$0.53^{+0.11}_{-0.10}$	1.14 (98)	0.98
25	$4.05^{+0.36}_{-0.34}$	$0.23^{+0.09}_{-0.08}$	0.50 ± 0.03	0.76 ± 0.04	$5.7^{+1.9}_{-1.6}$	$8.7^{+0.4}_{-0.1}$	$50.9^{+1.7}_{-1.5}$	6.0 fix#	$0.70^{+0.21}_{-0.19}$	1.43 (99)	0.75
26	$4.59^{+0.36}_{-0.35}$	0.23 ± 0.08	0.50 ± 0.03	$0.84^{+0.05}_{-0.04}$	$3.6^{+1.3}_{-1.1}$	$9.4^{+0.7}_{-0.8}$	$51.1^{+2.0}_{-1.8}$	6.0 fix#	$0.62^{+0.18}_{-0.19}$	1.27 (99)	0.68

* All errors represent the 90% confidence limits of the statistical uncertainties.
† Units in photons s^{-1} cm^{-2}.
‡ Units in photons s^{-1} cm^{-2} keV^{-1} at 1 keV.
§ X-ray luminosity in 3–100 keV in units of 10^{37} erg s^{-1}.
‖ HEXTE standard data are used. [HEXTE science data are used for other days.]
The width is fixed.
** Suzaku data. All others are from RXTE data.

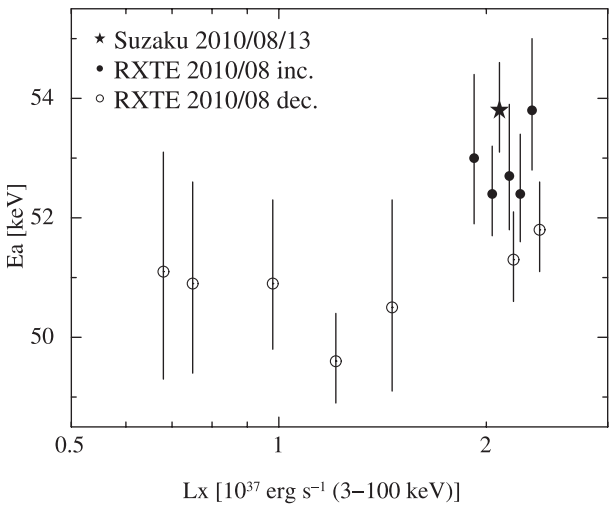

Fig. 4. Relation between the CRSF energy and the 3–100 keV X-ray luminosity during the 2010 August outburst. Data points obtained from the RXTE observations of increasing and decreasing phases, and the Suzaku observation are marked with filled circles, open circles, and a star, respectively. The vertical error bars represent the 90% confidence limits of the statistical uncertainty, obtained from the model fits.

the CRSF feature in the spectra taken on August 15 and 21. Thus, the resonance energy appears to have really changed between the two data sets.

Figure 4 plots the relation between the the CRSF energy and the 3–100 keV luminosity, estimated from the best-fit spectral models. The results allow at least two alternative interpretations. One is that the the CRSF energy depends positively on the X-ray luminosity. The other is that the CRSF energy splits into two regimes, $\sim$50 keV and $\sim$54 keV, depending possibly on the outburst phase (e.g., Caballero et al. 2008).

4. Discussion

We analyzed the broadband X-ray (3–130 keV) spectra of GX 304−1 obtained by RXTE and Suzaku, in ToO observations covering the two outbursts in 2010 detected by MAXI. A signature of CRSF was discovered at 54 keV from both the RXTE and the Suzaku data taken on August 13. It is the first detection of the CRSF from this source (Mihara et al. 2010b). Sakamoto et al. (2010) reported a Swift-BAT confirmation of the CRSF at around 50 keV from the spectrum accumulating data from August 12 to 17.

The CRSF energy of 54 keV exceeds that of A 0535+26 ($\sim$45 keV: Terada et al. 2006), and becomes the highest among the X-ray binary pulsars whose CRSF parameters are well determined. The surface magnetic field strength is estimated to be $4.7 \times 10^{12}\ (1 + z_{\rm g})$ G, where $z_{\rm g}$ represents the gravitational redshift. Makishima et al. (1999) examined the relation between the magnetic-field strength estimated from the CRSF and the pulsation period in X-ray binary pulsars, and discussed a group of "slow rotators"; represented by such sources as Vela X-1 and GX 301−2, these objects have much longer pulsation periods than would be expected if they were in rotational equilibria. The obtained field strength of 4.7×10^{12} G, and the pulsation period of 275.46 s measured during the Suzaku observation, place GX 304−1 just in the range of the typical slow rotators.

We performed spectral analysis of the RXTE data covering

the outburst in 2010 August on an almost daily basis. The CRSF has also been confirmed in 10 RXTE observations in which the source was sufficiently bright. Therefore, the CRSF is a persistent effect of this object. However, the CRSF energy was observed to vary, either in a positive correlation with the luminosity, or in a bimodal manner with $E_{\rm a} \sim 50\,{\rm keV}$ and $E_{\rm a} \sim 54\,{\rm keV}$.

Variations of the CRSF energy during a single outburst have been observed from 4U 0115+63 (Mihara et al. 1998, 2004; Nakajima et al. 2006) and X 0331+53 (V 0332+53) (Mowlavi et al. 2006; Tsygankov et al. 2006; Nakajima et al. 2010). However, in contrast to the behavior of GX 304−1 revealed in the present study, these two objects show negative correlations, that the CRSF energy decreases as the luminosity increases. The negative correlation can be explained by presuming that the cyclotron-scattering photosphere becomes higher when the accretion rate increased in the super-Eddington accretion regime (Mihara et al. 1998).

A positive correlation between the CRSF energy and the luminosity has been seen in the long-term behavior of Her X-1 over multiple outbursts (Gruber et al. 2001; Staubert et al. 2007). In addition, different CRSF energies were measured between two orbital phases in GX 301−2 (La Barbera et al. 2005). This behavior is expected in sub-Eddington accretion, where the cyclotron-scattering photosphere is lowered by the dynamical pressure of the accretion (Staubert et al. 2007). The observed behavior of GX 304−1, if interpreted as showing a positive dependence of $E_{\rm a}$ on the luminosity, may be a manifestation of the same effects, and regarded as the first example that the relation was observed in a single outburst. Indeed, the fraction of the CRSF-energy change, $\Delta E_{\rm a}/E_{\rm a} \sim 6\%$, is similar to that observed in Her X-1, and reasonably agrees with that of the quantitative estimate in these situations in Staubert et al. (2007).

A bimodal change in the CRSF energy was observed from A 0535+26 by Caballero et al. (2008); they measured the resonance energy at ∼46 keV in the 2005 outburst, and at ∼54 keV during its pre-putburst, even though the luminosity was comparable on the two occasions. Postnov et al. (2008) interpreted this effect in terms of magnetospheric instabilities between the accretion disk and the neutron-star magnetosphere at the onset of accretion. The same scenario may also apply to our figure 4, if it is interpreted as representing two typical values of $E_{\rm a}$.

Since the mission started on 2010 August 15, MAXI detected four X-ray outbursts from GX 304−1 by 132.5-day intervals. As reported by Manousakis et al. (2008), this confirmed the recurrence of the source activities after 28 years of X-ray disappearance. The source may have returned to the active state, such that it had been in until 1980. We urge continuous monitoring of this source, and follow-up observations of outbursts with hard X-ray instruments for further studies of the CRSF behaviors.

This research was partially supported by the Ministry of Education, Culture, Sports, Science and Technology (MEXT), Grant-in-Aid for Science Research (A) 20244015 and for Young Scientists (B) 21740140.

References

Caballero, I., et al. 2008, A&A, 480, L17
Coburn, W., Heindl, W. A., Rothschild, R. E., Gruber, D. E., Kreykenbohm, I., Wilms, J., Kretschmar, P., & Staubert, R. 2002, ApJ, 580, 394
Fukazawa, Y., et al. 2009, PASJ, 61, S17
Gruber, D. E., Heindl, W. A., Rothschild, R. E., Coburn, W., Staubert, R., Kreykenbohm, I., & Wilms, J. 2001, ApJ, 562, 499
Huckle, H. E., Mason, K. O., White, N. E., Sanford, P. W., Maraschi, L., Tarenghi, M., & Tapia, S. 1977, MNRAS, 180, 21
Jahoda, K., Markwardt, C. B., Radeva, Y., Rots, A. H., Stark, M. J., Swank, J. H., Strohmayer, T. E., & Zhang, W. 2006, ApJS, 163, 401
Kokubun, M., et al. 2007, PASJ, 59, S53
Koyama, K., et al. 2007, PASJ, 59, S23
Krimm, H. A., et al. 2010, Astron. Telegram, 2538
La Barbera, A., Segreto, A., Santangelo, A., Kreykenbohm, I., & Orlandini, M. 2005, A&A, 438, 617
Makishima, K., Mihara, T., Nagase, F., & Tanaka, Y. 1999, ApJ, 525, 978
Manousakis, A., et al. 2008, Astron. Telegram, 1613
Mason, K. O., Murdin, P. G., Parkes, G. E., & Visvanathan, N. 1978, MNRAS, 184, 45
Matsuoka, M., et al. 2009, PASJ, 61, 999
McClintock, J. E., Rappaport, S. A., Nugent, J. J., & Li, F. K. 1977, ApJ, 216, L15
McClintock, J. E., Ricker, G. R., & Lewin, W. H. G. 1971, ApJ, 166, L73
Menzies, J. 1981, MNRAS, 195, 67
Mihara, T. 1995, PhD thesis, The University of Tokyo
Mihara, T., et al. 1990, Nature, 346, 250
Mihara, T., et al. 2010a, Astron. Telegram, 2779
Mihara, T., et al. 2011, PASJ, 63, S623
Mihara, T., Makishima, K., & Nagase, F. 1998, Adv. Space Res., 22, 987
Mihara, T., Makishima, K., & Nagase, F. 2004, ApJ, 610, 390
Mihara, T., Yamamoto, T., Sugizaki, M., Yamaoka, K., & the MAXI team 2010b, Astron. Telegram, 2796
Mowlavi, N., et al. 2006, A&A, 451, 187
Nakajima, M., Mihara, T., & Makishima, K. 2010, ApJ, 710, 1755
Nakajima, M., Mihara, T., Makishima, K., & Niko, H. 2006, ApJ, 646, 1125
Parkes, G. E., Murdin, P. G., & Mason, K. O. 1980, MNRAS, 190, 537
Pietsch, W., Collmar, W., Gottwald, M., Kahabka, P., & Ögelman, H. 1986, A&A, 163, 93
Postnov, K., Staubert, R., Santangelo, A., Klochkov, D., Kretschmar, P., & Caballero, I. 2008, A&A, 480, L21
Priedhorsky, W. C., & Terrell, J. 1983, ApJ, 273, 709
Ricker, G. R., McClintock, J. E., Gerassimenko, M., & Lewin, W. H. G. 1973, ApJ, 184, 237
Rothschild, R. E., et al. 1998, ApJ, 496, 538
Sakamoto, T., et al. 2010, Astron. Telegram, 2815
Staubert, R., Shakura, N. I., Postnov, K., Wilms, J., Rothschild, R. E., Coburn, W., Rodina, L., & Klochkov, D. 2007, A&A, 465, L25
Sugizaki, M., et al. 2011, PASJ, 63, S635

Takahashi, T., et al. 2007, PASJ, 59, S35
Terada, Y., et al. 2006, ApJ, 648, L139
Thomas, R. M., Morton, D. C., & Murdin, P. G. 1979, MNRAS, 188, 19
Trümper, J., Pietsch, W., Reppin, C., Voges, W., Staubert, R., & Kendziorra, E. 1978, ApJ, 219, L105
Tsygankov, S. S., Lutovinov, A. A., Churazov, E. M., & Sunyaev, R. A. 2006, MNRAS, 371, 19
White, N. E., Swank, J. H., & Holt, S. S. 1983, ApJ, 270, 711
Yamamoto, T., et al. 2009, Astron. Telegram, 2297